Downloaded from UvA-DARE, the institutional repository of the University of Amsterdam (UvA)
http://hdl.handle.net/11245/2.26304

File ID uvapub:26304
Filename 119589y.pdf
Version unknown

SOURCE (OR PART OF THE FOLLOWING SOURCE):
Type article - letter to the editor
Title The X-ray spectra of the flaring and quiescent states of AT Microscopii observed by XMM-Newton
Author A.J.J. Raassen
Faculty FNWI: Astronomical Institute Anton Pannekoek (IAP)
Year 2003

FULL BIBLIOGRAPHIC DETAILS:
http://hdl.handle.net/11245/1.216694

Copyright

It is not permitted to download or to forward/distribute the text or part of it without the consent of the author(s) and/or copyright holder(s), other than for strictly personal, individual use.

UvA-DARE is a service provided by the library of the University of Amsterdam (http://dare.uva.nl)
(pagedate: 2014-08-15)

A&A 411, 509–515 (2003)
DOI: 10.1051/0004-6361:20031389
© ESO 2003

Astronomy & Astrophysics

The X-ray spectra of the flaring and quiescent states of AT Microscopii observed by XMM-Newton⋆

A. J. J. Raassen[1,2], R. Mewe[1], M. Audard[3], and M. Güdel[4]

[1] SRON National Institute for Space Research, Sorbonnelaan 2, 3584 CA Utrecht, The Netherlands
[2] Astronomical Institute "Anton Pannekoek", Kruislaan 403, 1098 SJ Amsterdam, The Netherlands
[3] Columbia Astrophysics Laboratory, Mail code 5247, 550 West 120th Street, New York, NY 10027, USA
[4] Paul Scherrer Institut, Würenlingen & Villigen, 5232 Villigen PSI, Switzerland

Received 3 February 2003 / Accepted 29 August 2003

Abstract. The X-ray spectrum of the late-type M-dwarf binary AT Mic (dM4.5e+dM4.5e) is observed in the wavelength range 1–40 Å by means of RGS and EPIC-MOS on board XMM-Newton. During the exposure a flare occured. We have performed a 3-temperature fit and a DEM-modeling to the flaring and quiescent part of the spectrum. We report the coronal temperature distribution, emission measures, and abundances of the flaring and quiescent state of this bright X-ray source. The temperature range stretches from about 1 to 60 MK. The total volume emission measure in this temperature interval is $\sim 12.2 \times 10^{51}$ cm^{-3} for the quiescent state and $\sim 19.5 \times 10^{51}$ cm^{-3} for the flare state. This difference is due to the contribution of the hot temperature component. The high-resolution spectrum of AT Mic, obtained by RGS, is dominated by the H- and He-like transitions of C, N, O, and Ne and by Fe XVII lines, produced by the plasma with temperatures from 1 to 10 MK. The EPIC-MOS spectrum below 10 Å shows H- and He-like Ne, Si and the iron K-shell transitions. They are produced by the hot component (30 MK). The iron K-shell is more prominent in the flare state. The abundance pattern in the quiescent state of AT Mic shows the depletion of low-FIP elements relative to high-FIP elements, indicating the presence of an I(nverse)FIP effect in this active star. In the flare state, however, some flattening of this IFIP effect is present.

Key words. stars: individual: AT Mic – stars: coronae – stars: late-type – missions: – XMM-Newton

1. Introduction

Hot outer atmospheres (coronae) are very common for relatively cool stars in the spectral classes F–M. Many of these coronae are characterized by temperatures up to about 20 MK and densities $n_e \gtrsim 10^{10}$ cm^{-3}. It was already known that the coronae of many stars are different from the solar corona (e.g., reviews by Pallavicini 1989; Mewe 1991). The heating mechanism of these coronae, however, is still not well understood. A variety of possible explanations is present, such as, convection zones with MHD waves transfering energy from the photosphere into the corona, large flares heating plasma by reconnection, or a large number of continuously heating micro- and nanoflares. High-resolution spectroscopy of stellar systems available from Chandra (Brinkman et al. 2000; Canizares et al. 2000) and XMM-Newton (Brinkman et al. 2001) offers the possibility to study the coronal spectra in great detail and to determine various coronal quantities, such as densities, temperatures, abundances, emission measures, and line ratios, during the flaring states as well as during the quiescent state.

Late-type stars (M and K dwarfs) show more magnetic activity and higher coronal temperatures than the Sun, characterized by flaring (Pettersen 1989) in the optical, UV, X-ray and radio wavelengths (Pallavicini et al. 1990). To understand the mechanisms that underly the high temperatures and the variety of densities, emission measures, and abundance values observed in coronal systems, the X-ray spectra of stars of type F−M are investigated, especially focused on stars with flare activity. In very active stars, however, the "quiescent state" might be produced by a superposition of flare decays and microflares rather than by a real quiescent coronal plasma. Here we present the investigation of the active M-type binary star AT Mic (dM4.5+dM4.5) at a distance of 10.22 pc (Perryman et al. 1997). Both components are known to flare frequently (Joy & Wilson 1949). Large optical flares were observed by García-Alvarez et al. (2002), while X-ray flares were studied e.g., by HEAO-1 (Kahn et al. 1979) and by EXOSAT (Pallavicini et al. 1990). The quiescent corona was observed by EUVE (Monsignori Fossi et al. 1995).

2. Observations

The X-ray spectrum of AT Mic was observed by RGS and EPIC-MOS on board XMM-Newton on 14 October 2000

Send offprint requests to: A. J. J. Raassen,
e-mail: a.j.j.raassen@sron.nl

⋆ Based on observations obtained with *XMM-Newton*, an ESA scienc mission with instruments and contributions directly funded by ESA Member States and the USA (NASA).

Table 1. Observation log of the data of AT Mic.

Instrument	Filter	Mode	Date-obs-start	Date-obs-end	Performed duration (s)
MOS1	Medium	Small Window	2000-10-16T00:27:48	2000-10-16T07:34:02	25394
MOS2	Medium	Timing	2000-10-16T00:38:15	2000-10-16T07:34:29	24794
pn	Medium	Small Window	2000-10-16T00:41:50	2000-10-16T07:41:13	25103
RGS1	None	Spec+Q	2000-10-16T00:19:12	2000-10-16T08:11:48	28254
RGS2	None	Spec+Q	2000-10-16T00:19:12	2000-10-16T08:11:48	28254

during revolution 156. The observation log of the data is presented in Table 1.

The data were processed by means of the XMM-Newton SAS version 5.3.3 (June 2002). The exposure time was 28.3 ks for RGS and 25.4 ks for EPIC-MOS1, of which 19.0 ks were free of solar flare proton "pollution" applying the criterion that the latter's count rate should be $\lesssim$0.35 c/s. For RGS the first-order net spectra were extracted by including 95% of the cross dispersion PSF (xpsfincl = 95 in rgsproc) and the background spectra were extracted by excluding 98% (xpsfexcl = 98 in rgsproc).

The RGS spectral resolution is $\Delta\lambda \sim 0.07$ Å (FWHM), with a maximum effective area of about 140 cm^2 around 15 Å. The wavelength uncertainty is 7–8 mÅ. The total RGS spectrum runs from 5 to 37 Å. Only the range from 8 to 37 Å was used. For EPIC-MOS1, which observed in the small-window mode, we extracted the spectrum by means of a circle centered around the source with a radius of 40 arcsec. The background was obtained by applying the same circle in a source free area at another CCD. The same SAS version was used to construct response matrix and ancillary response files. The range from 1 to 14 Å was used. EPIC-MOS2 was operating in the timing mode. For more instrumental details on RGS and EPIC-MOS see den Herder et al. (2001) and Turner et al. (2001), respectively. The pn data were used to produce a lightcurve only.

3. Analysis

3.1. Quiescence versus flaring state

Based on the lightcurves obtained with RGS, EPIC-MOS and pn (see Fig. 1) we have concluded that AT Mic was flaring several times during our observations. A period of about 2.9 ks related to the most prominent flare was extracted from the GTI table as flare state, leaving a pseudo-quiescent part of 14.1 ks. Three other weak flares can be seen in Fig. 1. However, they do not dominate and have therefore not been flagged as flares in the further spectral analysis. From Fig. 1 we notice that the top of the flare is not constant, but shows small variations, which seem to be periodic. However, these time intervals are too short to allow for individual spectral analysis.

The observed spectra are shown in Fig. 2 for the quiescent (top) and flaring (bottom) state. As can be seen from Fig. 2, EPIC-MOS has a low resolution, but a high sensitivity compared to RGS. Due to the short exposure time of the flaring state the signal/noise ratio is lower for that spectrum. For both states shown in Fig. 2 it is clear that the X-ray spectrum obtained by RGS in the wavelength range from 5 to 37 Å is

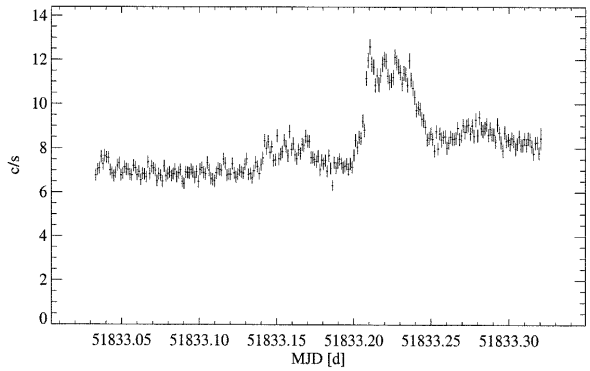

Fig. 1. Lightcurve of AT Mic, observed with pn.

dominated by H- and He-like transitions of C, N, O, and Ne and by Fe XVII lines, while the low-resolution EPIC-MOS spectrum shows the Fe K-shell transitions around 1.9 Å and the H- and He-like transitions of Ne and Si. The Fe K-shell feature (see also Table 4) as well as the continuum appear more prominent in the spectrum of the flaring state (bottom panel) than in that of the quiescent state.

3.1.1. Multi-temperature fitting

The data of the quiescent state and the flaring state have been fitted with a 3-T Collisional Ionization Equilibrium model using the SPEX code (Kaastra et al. 1996a) in combination with an updated version of MEKAL (Mewe et al. 1995; Phillips et al. 1999). The MEKAL database is publicly available[1] as an extended list of fluxes of more than 5400 spectral lines. Figure 3 shows the comparison of the quiescent spectrum with the best-fit model. The fits have been performed by attaching the errors to the data ("fit weight data"), given in the columns "data", and by attaching the errors to the model ("fit weight model"), given in the columns "model". In the abstract the values from the "data fit" are given.

Table 2 shows the 3 temperatures, the emission measures in 10^{51} cm^{-3}, and abundances together with their standard deviations within parentheses. The abundances are normalized to their corresponding solar photospheric values (Anders & Grevesse 1989), except for iron and oxygen. For Fe we have changed the value of log $A_{\rm Fe}$ from 7.67 (Anders & Grevesse 1989) to 7.51 (Grevesse & Sauval 1998, 1999). For oxygen we used the new value given by

[1] `http://www.sron.nl/divisions/hea/spex/version1.10/line/line_new.ps.gz`

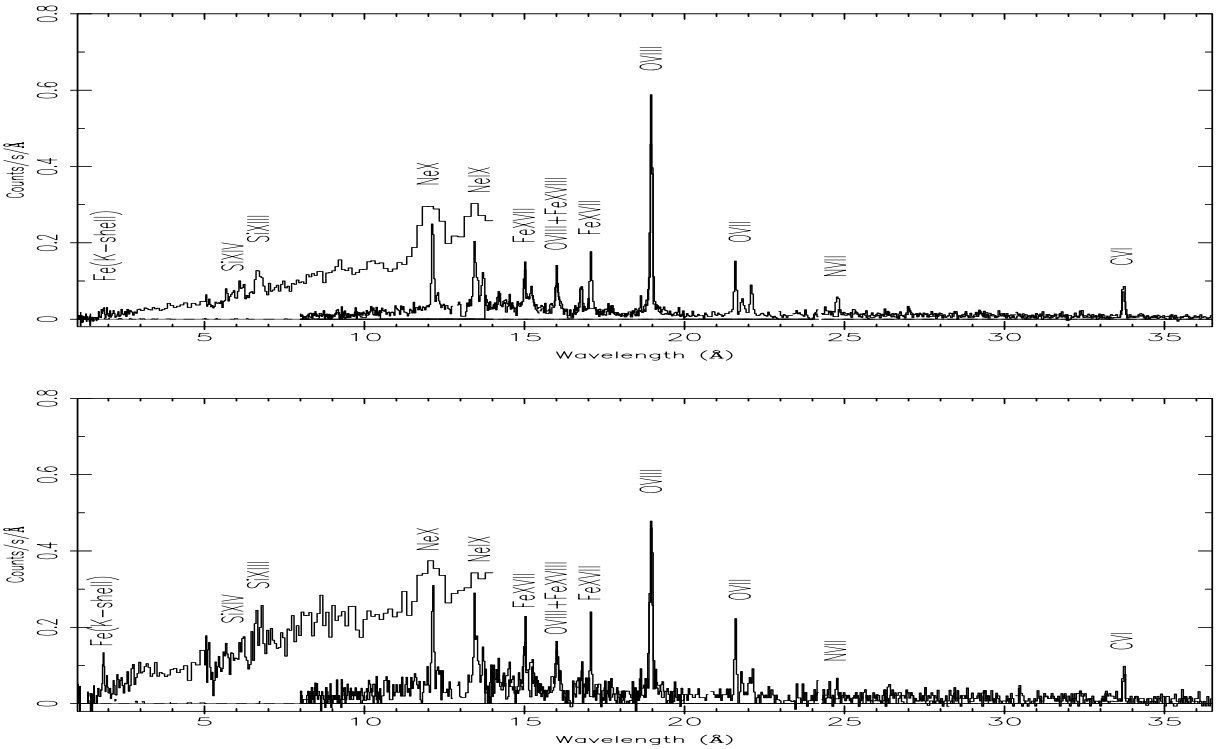

Fig. 2. The spectra of AT Mic observed by RGS1, RGS2 and EPIC-MOS in the wavelength region from 1 to 37 Å. The upper panel shows the quiescent state, while the lower panel shows the flaring state.

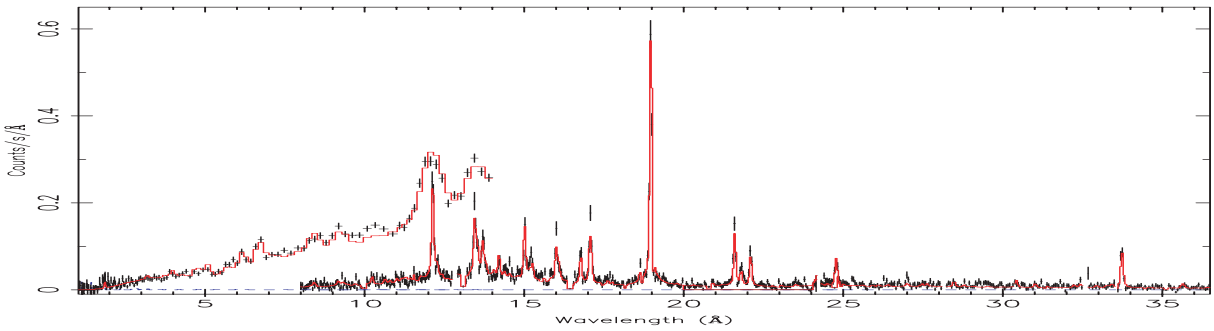

Fig. 3. Comparison of the AT Mic quiescent spectrum (see Fig. 2a) with the best-fit model (unbroken line).

Allende Prieto & Lambert (2001) (log A_O = 8.69 instead of 8.93). Here log A_{Fe} and log A_O is the logarithm of the Fe- and O-abundance relative to log A_H = 12.0.

The temperatures in Table 2 cover a range from 3 to 35 MK. It turns out that the line spectrum is mainly produced by the EM related to T_1 = 3 MK and to T_2 = 8 MK, while the hot component T_3 > 20 MK contributes to the continuum below 10 Å and the Fe K-shell lines in the EPIC-MOS observation. This is especially true for the flaring state. A fourth cool component (1 MK) is possible but not well constrained. This cool component is only related to the C VI line (influencing the C abundance) and very weakly coupled to the continuum. The total emission measure of the three components is 12.2(.5) × 10^{51} cm^{-3} for the quiescent state and 19.5(.8) × 10^{51} cm^{-3} for the flare state. Based on EUVE observations, Monsignori Fossi et al. (1995) have determined an emission measure maximum of about 3 × 10^{51} cm^{-3} around 10 MK (their Fig. 5), detecting only the emission measure related to our second temperature component at T_2 (7.9 MK).

When fitting the O VII lines a slight increase of the electron density n_e is noticed, from the quiescent state to the flaring state. However, this increase is not statistically significant.

In the energy interval from 0.3 to 10 keV the X-ray luminoscity L_x is 2.13(.08) × 10^{29} erg/s for the quiescent state and 3.63(.22) × 10^{29} erg/s for the flaring state. These values are averages of the "data" and "model" fit. Pallavicini et al. (1990) observed AT Mic with EXOSAT (ME 1–10 keV detector) during quiescence and during a flare. The quiescent X-ray luminosity was measured to be 1.8 × 10^{29} erg/s (Table 5 of Pallavicini et al. 1990) in agreement with our value. However, they observed a larger flare, but with the same temperature as ours.

Table 2. Multi-temperature fitting to the quiescent and flaring state of AT Mic; 1σ uncertainties are given in the last digits in parentheses.

PARAMETER	QUIESCENT[a]		FLARING	
	data[b]	model[b]	data	model
log $N_{\rm H}$ [cm^{-2}]	18.3[c]	18.3[c]	18.3[c]	18.3[c]
T_1 [MK]	3.16(.10)	2.94(.10)	2.91(.17)	2.71(.20)
T_2 [MK]	7.77(.13)	7.54(.14)	8.57(.34)	7.80(.27)
T_3 [MK]	23.0(1.0)	27.9(2.3)	33.9(3.2)	32.8(5.1)
EM_1 [10^{51} cm^{-3}]	2.34(.16)	3.86(.41)	2.71(.31)	4.95(1.3)
EM_2 [10^{51} cm^{-3}]	4.85(.26)	8.58(.93)	4.27(.42)	10.9(4.0)
EM_3 [10^{51} cm^{-3}]	4.99(.20)	5.51(.44)	12.47(.61)	16.5(1.9)
$EM_{\rm total}$[10^{51} cm^{-3}]	12.2(.5)	17.8(1.1)	19.5(.8)	32.4(4.6)
$n_{\rm e}$(O) [10^{10} cm^{-3}][d]	1.9(1.5)	1.4(1.4)	4(−3,+5)	3(−3,+4)
$L_{\rm x}$ [10^{29} erg/s][e]	2.05(.08)	2.26(.14)	3.54(.15)	3.98(.57)
Mg/O 7.65 eV	0.51(.06)	0.44(.09)	1.00(.22)	0.68(.28)
Fe/O 7.87 eV	0.34(.02)	0.31(.05)	0.56(.04)	0.45(.16)
Si/O 8.15 eV	0.60(.06)	0.69(.11)	0.72(.22)	0.68(28)
C/O 11.26 eV	1.00(.10)	1.01(.19)	0.83(.21)	0.84(.30)
O/O 13.62 eV	1.00(.05)	1.00(.14)	1.00(.10)	1.00(.25)
N/O 14.53 eV	0.86(.09)	0.73(.16)	0.58(.27)	0.51(.31)
Ne/O 21.56 eV	1.52(.08)	1.48(.20)	1.90(.21)	1.50(.49)
O/H 13.62 eV	1.57(.05)	0.96(.09)	1.43(.10)	0.71(.13)
$EM_{\rm total}\times$ O/H	19.2(1.0)	17.1(2.0)	27.9(2.3)	23.0(5.3)
χ^2/d.o.f.	1.1	1.4	0.60	1.10

[a] Based on good time interval (with low solar proton flux) and excluding the stellar flare (see Fig. 5).
[b] Data stands for "fit weight data" and model stands for "fit weight model".
[c] Fixed at literature value from Monsignori Fossi et al. (1995).
[d] Based on O VII lines only.
[e] In the 0.3–10 keV energy interval.

The abundances have been determined by fitting to the spectrum as a whole. As a check, whether a large scatter exists between different lines of the same element, abundances were also fitted to isolated individual lines, keeping temperatures, emission measures and other abundances fixed at the values from the global fit (Table 2). In this way blends have been taken into account. Due to the weak continuum the absolute abundances cannot be coupled accurately to the continuum and therefore they are strongly anticorrelated with the emission measure. This means that if one quantity increases the other decreases and vice versa. This is clear from comparing the $EM_{\rm total}$ from the "data fit" with that from the "model fit" and by comparing the absolute oxygen abundance (O/H) in these columns. The product $EM_{\rm total}\times$ O/H, however, is more stable. For this reason the abundance *ratios*, normalized to oxygen, are more robust. Oxygen was chosen for its low relative standard deviation, thanks to the strong O VIII and O VII lines. For the (less active) solar corona Feldman et al. (1992) discussed the presence of a First Ionization Potential (FIP) effect. This effect implies that elements with a low value of the first ionization potential (e.g., $\lesssim$10 eV) show enhanced coronal abundances relative to photospheric values. However, the abundance ratios of the low-FIP elements Mg, Si, and Fe are relatively low in AT Mic, indicating an *inverse* FIP-effect (IFIP). Similar IFIP effects were observed by Brinkman et al. (2001), Güdel et al. (2001), Audard et al. (2002) and Audard et al. (2003) for other active late-type stars. This IFIP effect is illustrated in Fig. 4 (top), which shows the trend of an *increasing* abundance ratio with increasing FIP for the quiescent state. In the bottom panel the same quantities are shown for the flaring state. However, due to the short time interval all quantities determined in the flare spectrum have large statistical uncertainties. The poor signal-to-noise ratio of the flaring state data is also reflected in the "too good" χ^2/d.o.f. of the multitemperature fit. This suggests an overestimate for the errors in this low count rate spectrum. For that reason the fits have also been performed, attaching the errors to the model, resulting in reasonable χ^2/d.o.f.-values.

Table 3. Ratio between the scaled abundance values of the flaring and quiescent state from Table 2.

Parameter	flaring/quiescent
Mg/O 7.65 eV	1.75(.42)
Fe/O 7.87 eV	1.63(.20)
Si/O 8.15 eV	1.11(.30)
C/O 11.26 eV	0.83(.20)
O/O 13.62 eV	1.00(.11)
N/O 14.53 eV	0.68(.27)
Ne/O 21.56 eV	1.19(.17)

Comparing the quiescent state with the flaring state some flattening of this IFIP effect for the low FIP elements (Fe and Mg) is noticed in the flaring state. This is shown in Table 3 and Fig. 4c, in which the ratios between the A/O values of the flaring and quiescent state are given. The values used in Table 3 and Fig. 4 are averages between "data" and "model" values. Si seems not to be affected by the difference between the flaring state and the quiescent state. In the solar corona the enhancement of the low-FIP elements starts from 10 eV down. Results in Table 3 and Fig. 4c may indicate a value lower than 10 eV below which the elemental abundances are influenced. Such a shift might be related to the lower surface temperature of AT Mic.

3.2. DEM-modeling

To show the smooth connection between the three separated temperature components of the multi-temperature fit (Table 2) we have performed a DEM-modeling of the RGS and EPIC-MOS spectra of AT Mic in the quiescent and flaring state, applying the regularization method and the polynomial method present in the SPEX-code (see Kaastra et al. 1996b). In this DEM-modeling the abundance ratios given in Table 2 have been used in combination with an O/H value of 1.57 for the quiescent state and 1.39 for the flare state. The emission measures $EM = n_{\rm e}n_{\rm H}V$ (per logarithmic temperature bin) of the corona of AT Mic are shown in Figs. 5a,b for both states. The emission measure is distributed from ~1 up to about 60 MK for the

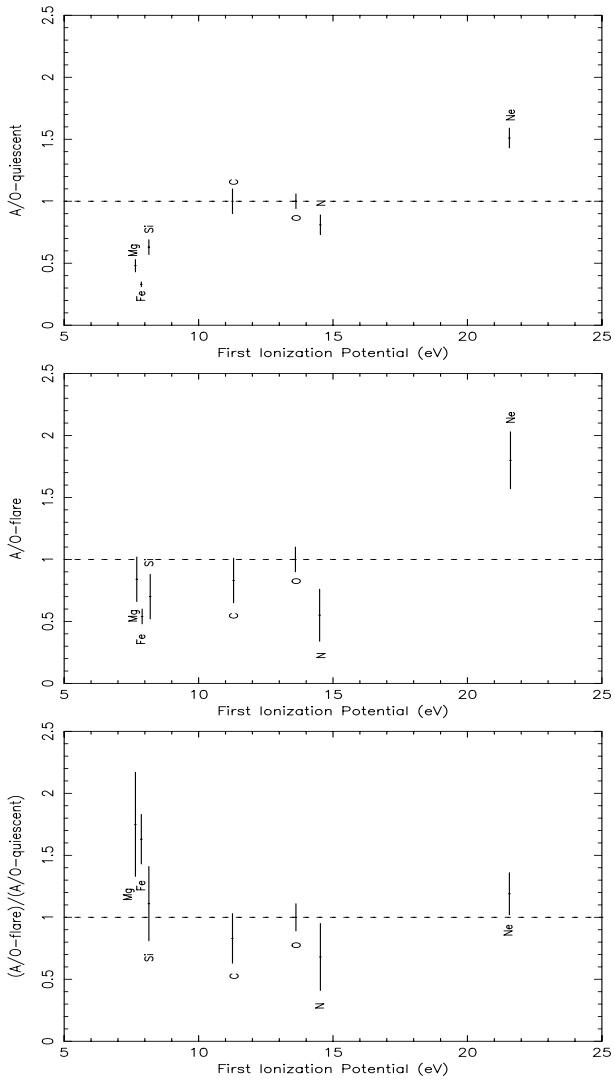

Fig. 4. Abundance ratio (A/O) versus First Ionization Potential, relative to solar photospheric values by Anders & Grevesse (1989) and Grevesse & Sauval (1998 and 1999) and with oxygen values from Allende Prieto & Lambert (2001) for the quiescent state (top) and the flaring state (middle). The bottom panel shows the ratio between the A/O of the flaring state and the A/O of the quiescent state (Table 3).

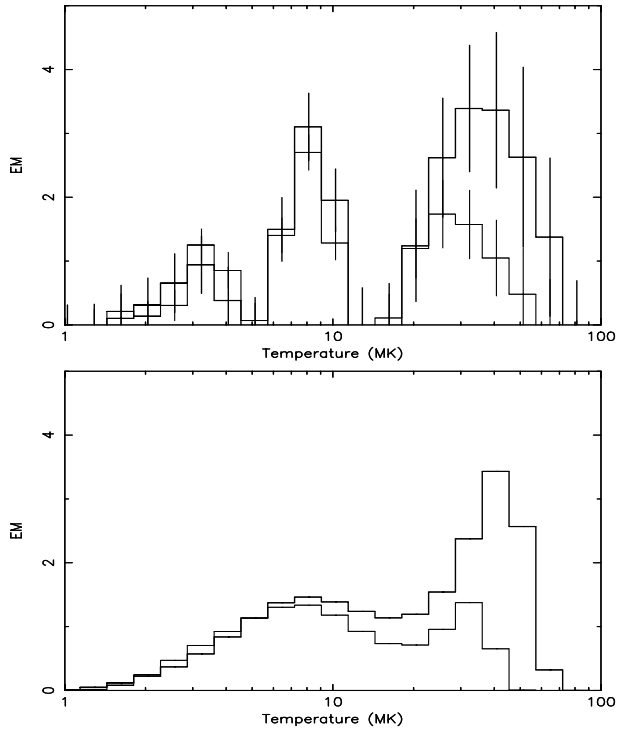

Fig. 5. DEM modeling of the flare spectrum (bold) and quiescent spectrum (weak) of AT Mic in units 10^{51} cm^{-3}, using the regularization method (top panel). The bottom panel shows the same for the polynomial method of order 9.

flare state. The DEM distribution agrees with the three temperature components from the multi-temperature fit if we take into account the uncertainties corresponding to the standard deviations.

Table 2 and Fig. 5 show the increase of the emission measure and a shift to higher temperatures for the hot EM (40 MK) during the flare state (bold) compared to the quiescent state (weak). The emission measure below 10 MK is the same for the quiescent and flaring state.

3.3. Individual lines

The more prominent lines of the RGS spectrum have been measured individually. Delta functions were folded through the instrumental response matrix in order to derive integrated line fluxes. No additional width to the delta functions was needed to fit the line shapes. A "constant" level was adjusted to take into account the real continuum or the "pseudo-continuum", created by the overlap of numerous weak lines.

The line fluxes are compared between the quiescent and flaring state (Table 4). Especially the flux difference of the Fe XXV line at 1.84 Å between the two states is clear. This line has a far higher flux in the flare state than in the quiescent state. The same is true for other highly ionized (hot) ions, such as Si XIV, Si XIII, Fe XIX, Fe XVIII, and Fe XVII. However, for these ions the effect is less significant.

3.4. Density measurement

The three He-like transitions, consisting of the resonance line (r) 1s^2 ^{1}S$_0$–1s2p ^{1}P$_1$, the intercombination line (i) 1s^2 ^{1}S$_0$–1s2p ^{3}P$_1$, and the forbidden line (f) 1s^2 ^{1}S$_0$–1s2s ^{3}S$_1$ are density- and temperature-dependent (e.g., Gabriel & Jordan 1969). At increasing electron density the low-lying 1s2s ^{3}S$_1$ level will be depopulated in favour of the 1s2p ^{3}P$_1$ level, resulting in a decrease of the intensity of the forbidden line and an increase of the intercombination line. This makes the ratio $R = f/i$ a valuable diagnostic tool for densities. The He-like lines of oxygen are well separated, although the intercombination line in the quiescent spectrum is affected by an innershell transition in O VI (see Fig. 6). These lines at 21.602 Å (r), 21.802 Å (i) and 22.101 Å (f) have been used to obtain temperature and density values from the G- and R-ratio using the tables by Porquet et al. (2001). For representative temperatures around 3 MK, we derive electron densities of

Table 4. Observed line fluxes of the quiescent and flare spectra of AT Mic.

QUIESCENT		FLARING		LINE ID[a]	
λ(Å)	Flux[b]	λ(Å)	Flux[b]	λ(Å)	Ion
1.86(.05)[c]	0.06(.03)	1.84(.05)	0.42(.18)	1.85	Fe XXV
6.2(.2)[c]	0.22(.12)	6.2(.2)	0.67(.42)	6.182	Si XIV
6.7(.2)[c]	0.75(.13)	6.7(.2)	1.4(.8)	6.7	Si XIII
12.136(.005)	4.7(.5)	12.142(.009)	5.3(1.2)	12.134	Ne X
13.451(.005)	3.4(.4)	13.442(.018)	3.5(1.4)	13.447	Ne IX
13.533(.014)	1.0(.3)	13.521(.032)	2.4(1.4)	13.521	Fe XIX
				13.553	Ne IX
				13.670	Fe XIX
13.711(.014)	1.9(.3)	13.710(.018)	1.8(.8)	13.700	Ne IX
15.011(.009)	2.16(.31)	15.012(.017)	4.1(.9)	15.014	Fe XVII
16.008(.009)	1.73(.29)	16.017(.009)	2.7(.8)	16.007	O VIII
				16.078	Fe XVIII
16.763(.014)	1.20(.35)	16.791(.023)	1.9(1.0)	16.775	Fe XVII
17.050(f)	1.47(.37)	17.050(f)	1.6(.8)	17.055	Fe XVII
17.101(f)	1.30(.37)	17.101(f)	1.6(.9)	17.100	Fe XVII
18.655(.018)	0.53(.20)	18.645(0.46)	0.5(.5)	18.628	O VII
18.972(.007)	10.7(.7)	18.962(.006)	11.2(1.5)	18.969	O VIII
21.587(.009)	3.29(.61)	21.582(.018)	3.9(1.0)	21.602	O VII
21.789(.014)	0.64(.48)	21.800(.024)	1.4(.7)	21.801	O VII
21.846(.037)	0.72(.50)	—	—	21.845	O VI
22.085(.009)	1.49(.18)	22.086(.034)	1.8(.6)	22.101	O VII
24.781(.009)	1.07(.26)	24.779(.028)	1.1(.6)	24.781	N VII
33.718(.007)	3.14(.53)	33.736(.018)	2.8(1.2)	33.736	C VI

[a] Line identification from Kelly (1987).
[b] Measured flux in 10^{-4} photons/cm^2/s.
[c] Wavelengths and fluxes from EPIC-MOS.

$3 \pm 2 \times 10^{10}$ cm^{-3} for the quiescent state and $8^{+20}_{-7.5} \times 10^{10}$ cm^{-3} for the flaring state. Within the errors these values agree with those given in Table 2.

4. Conclusions

The X-ray spectrum of AT Mic obtained by RGS and EPIC-MOS is dominated by H- and He-like transitions of Ne, O, N, and C and by Fe XVII lines (RGS) and by H- and He-like transitions of Si and Mg and Fe K-shell transitions (EPIC-MOS).

The spectra correspond to a quiescent and a flaring state as was concluded from the observed light curve. The dominant temperatures and emission measures cover a broad temperature range from 1 up to about 60 MK. The total emission measure in this temperature domain is $\sim 12.2 \times 10^{51}$ cm^{-3} for the quiescent state and $\sim 19.5 \times 10^{51}$ cm^{-3} for the flaring state. Both values are obtained from the "fit weight data" fits.

From the O VII lines a density of $\sim 2 \times 10^{10}$ cm^{-3} is derived for the quiescent state and of $\sim 4 \times 10^{10}$ cm^{-3} for the flaring state. The density of the flaring state is somewhat higher, but due to the poor statistics this is not significant.

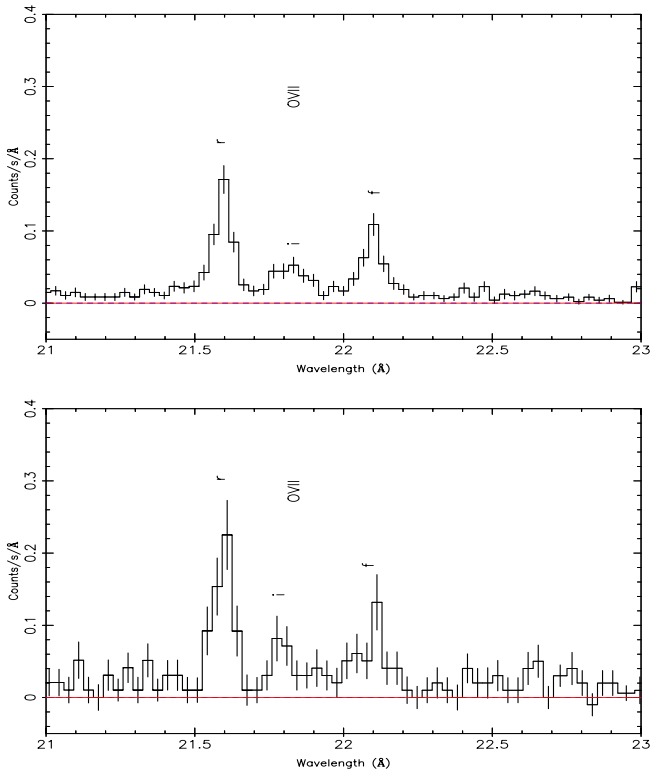

Fig. 6. The O VII lines of AT Mic observed by RGS1. The top panel shows the quiescent state, while the lower panel shows the flaring state.

Most line features of the RGS spectra are produced in the temperature range from 3–10 MK, dominated by quiescent emission. Lines from highly ionized atoms are enhanced in the flare state spectrum.

The abundance pattern in AT Mic shows the depletion of low-FIP elements (<10 eV) relative to high-FIP elements in the quiescent state. This indicates the presence of a possible IFIP effect in this active star, as has been shown for other active stars by Audard et al. (2002), Audard et al. (2003), Brinkman et al. (2001), Güdel et al. (2001), and Güdel et al. (2002). However, in the flare state this effect appears to be suppressed. This may imply that during the flare material from deeper layers with photosperic/chromospheric abundances is transported into the corona.

Acknowledgements. The SRON National Institute for Space Research is supported financially by NWO. The PSI group acknowledges support from the Swiss National Science Foundation (grant 2100-049343). MA acknowledges support from the Swiss National Science Foundation (fellowship 81EZ-67388).

References

Allende Prieto, C., & Lambert, D. L. 2001, ApJ, 556, L63
Anders, E., & Grevesse, N. 1989, Geochim. Cosmochim. Acta, 53, 197

Audard, M., Güdel, M., Sres, A., et al. 2002, in Stellar Coronae in the Chandra and XMM-Newton Era, ed. F. Favata, & J. J. Drake, ASP Conf. Ser., in press
Audard, M., Güdel, M., Sres, A., Raassen, A. J. J., & Mewe, R. 2003, A&A, 398, 1137
Brinkman, A. C., Gunsing, C. J. T., Kaastra, J. S., et al. 2000, ApJ, 530, L111
Brinkman, A. C., Behar, E., Güdel, M., et al. 2001, A&A, 365, L324
Canizares, C. R., Huenemoerder, D. P., Davis, D. S., et al. 2000, ApJ, 539, L41
Feldman, U., Mandelbaum, P., Seely, J. F., et al. 1992, ApJS, 81, 387
Gabriel, A. H., & Jordan, C. 1969, MNRAS, 145, 241
García-Alvarez, D., Jevremović, D., Doyle, J. G., & Butler, C. J. 2002, A&A, 383, 548
Grevesse, N., & Sauval, A. J. 1998, Space Sci. Rev., 85, 161
Grevesse, N., & Sauval, A. J. 1999, A&A, 347, 348
Güdel, M., Audard, M., Briggs, K., et al. 2001, A&A, 365, L336
Güdel, M., Audard, M., Smith, K. W., et al. 2002, ASP Conf. Ser., Cool Stars workshop, 12
den Herder, J. W., Brinkman, A. C., Kahn, S. M., et al. 2001, A&A, 365, L7
Joy, A. H., & Wilson, R. E. 1949, ApJ, 109, 231
Kaastra, J. S., Mewe, R., & Nieuwenhuijzen, H. 1996a, in UV and X-ray Spectroscopy of Astrophysical and Laboratory Plasmas, ed. K. Yamashita, & T. Watanabe (Tokyo: Universal Academy Press, Inc.), 411 (SPEX)
Kaastra, J. S., Mewe, R., Liedahl, D. A., et al. 1996b, A&A, 314, 547
Kahn, S. M., Linsky, J. L., Mason, K. O., et al. 1979, ApJ, 234, L107
Mewe, R. 1991, A&ARv, 3, 127
Mewe, R., Kaastra, J. S., & Liedahl, D. A. 1995, Legacy, 6, 16 (MEKAL)
Monsignori Fossi, B. C., Landini, M., & Drake, J. J. 1995, A&A, 302, 193
Pallavicini, R. 1989, A&ARv, 1, 177
Pallavicini, R., Tagliaferri, G., & Stella, L. 1990, A&A, 228, 403
Perryman, M. A. C., Lindegren, L., Kovalevsky, J., et al. 1997, A&A, 323, L49
Pettersen, B. R. 1989, Sol. Phys., 121, 299
Phillips, K. J. H., Mewe, R., Harra-Murnion, L. K., et al. 1999, A&AS, 138, 381
Porquet, D., Mewe, R., Dubau. J., et al. 2001, A&A, 376, 1113
Turner, M. J. L., Abbey, A., Arnaud, M., et al. 2001, A&A, 365, L27